nature photonics

LETTERS

PUBLISHED ONLINE: 14 SEPTEMBER 2014 | DOI: 10.1038/NPHOTON.2014.214

High photon flux table-top coherent extreme-ultraviolet source

Steffen Hädrich[1,2]*, Arno Klenke[1,2], Jan Rothhardt[1,2], Manuel Krebs[1], Armin Hoffmann[1], Oleg Pronin[3], Vladimir Pervak[3], Jens Limpert[1,2,4] and Andreas Tünnermann[1,2,4]

High harmonic generation (HHG) enables extreme-ultraviolet radiation with table-top set-ups[1]. Its exceptional properties, such as coherence and (sub)-femtosecond pulse durations, have led to a diversity of applications[1]. Some of these require a high photon flux and megahertz repetition rates, for example, to avoid space charge effects in photoelectron spectroscopy[2–4]. To date, this has only been achieved with enhancement cavities[5]. Here, we establish a novel route towards powerful HHG sources. By achieving phase-matched HHG of a megahertz fibre laser we generate a broad plateau (25 eV–40 eV) of strong harmonics, each containing more than 1×10^{12} photons s^{-1}, which constitutes an increase by more than one order of magnitude in that wavelength range[6–8]. The strongest harmonic (H25, 30 eV) has an average power of 143 μW (3×10^{13} photons s^{-1}). This concept will greatly advance and facilitate applications in photoelectron or coincidence spectroscopy[9], coherent diffractive imaging[10] or (multidimensional) surface science[2].

In the late 1980s, the first experiments on high harmonic generation (HHG) driven by intense pulsed lasers were performed[11,12]. The process rapidly attracted a great deal of attention because of its non-perturbative behaviour[12], its coherence[13], the potential for sub-femtosecond pulse trains[14] or isolated attosecond pulses[15], and its table-top set-up[12]. Today, significant efforts to further advance this still growing field are leading to an ever increasing demand for novel laser sources. The established laser technology for HHG is based on Ti:sapphire chirped pulse amplifiers, which deliver multi-millijoule, ultrashort (~25 fs) pulses with only several kilohertz of repetition rate at 800 nm. An increase in repetition rate to the megahertz level with increased photon flux (the number of photons per second per harmonic) would, for example, help to mitigate space charge effects in photoelectron spectroscopy[2–4], reduce integration times in coherent diffractive imaging[10] or increase the signal-to-noise ratio in general.

Inherently, increasing the repetition rate in HHG is associated with average power scaling of ultrashort-pulse lasers, which is challenging to realize. In this regard, the use of passive enhancement cavities (ECs), which coherently overlap pulses inside a high-finesse resonator, has been considered the most promising approach[5]. HHG is directly achieved inside the resonator, which requires an outcoupling mechanism by default. This latter requirement, as well as ionization-induced phase shifts, have been identified as the most severe limitations of enhancement factors (intra-cavity intensity), stability and accessible wavelength range[16]. A highest average power of ~200 μW in the 11th harmonic (12.7 eV) of enhanced 1,070 nm fibre lasers has been obtained with this approach, but with rapidly decreasing signal towards 30 eV (ref. 5). Recently, the use of ECs was extended to shorter wavelengths by demonstrating harmonics up to 100 eV and 5.3 μW in the 27th harmonic (32.5 eV)[6].

At the same time, the complementary approach of directly using high-repetition-rate lasers for HHG has been pursued. Although up to 20 MHz has been demonstrated, the attainable photon flux was orders of magnitude lower than that of ECs or traditional Ti:sapphire lasers, because phase matching was not achieved[17].

In this Letter we demonstrate phase-matched HHG of a nonlinear compressed fibre chirped pulse amplifier (FCPA), resulting in a conversion efficiency of more than 10^{-6} into a single harmonic at 30 eV. This demonstrates a new class of coherent extreme-ultraviolet sources where the average power in the 25–40 eV range is increased by more than one order of magnitude over previous systems[6–8].

HHG can be understood with a simple three-step model that describes the response of a single atom to a strong laser field[18]. The single-atom response to a certain intensity, that is, the dipole amplitude A_q, can be obtained quantum-mechanically[19] or modelled by empirical scaling laws[20]. The overall yield obtained in HHG, however, critically depends on macroscopic effects (phase matching), that is, the coherent build-up along the generation medium. The dipole amplitude A_q significantly increases with intensity, but at the same time the increased ionization fraction strongly influences the phase matching[1,21]. It has to be noted that the use of ultrashort laser pulses reduces the impact of ionization and allows the use of higher intensities[1], therefore increasing A_q. Ultimately, the signal build-up is limited by linear absorption of the harmonics in the generation medium itself[22].

For the present experiments we used an FCPA with subsequent nonlinear compression (see Methods). The system delivers laser pulses with 130–150 μJ of energy, a duration of ~30 fs (Fig. 1a) and variable repetition rates[23]. These pulses were focused to a focal spot diameter of 90 μm ($1/e^2$ intensity, Fig. 1b) inside a vacuum chamber containing gas jets (Fig. 1c) of different diameter. The generated harmonics and the remaining infrared light pass two SiO_2 surfaces (see Methods), reducing the average power of the driving laser to protect the following two aluminium filters (1 μm thickness) against damage. Subsequently, the harmonics are analysed with a flat-field grating-based spectrometer (see Methods). Optimization of the experimental parameters was carried out for xenon gas, as it has the lowest ionization potential and highest A_q of all noble gases. The intensity in the focal spot was reduced gradually from 1.5×10^{14} W cm^{-2} until blueshifting of the harmonics with increasing pressure disappeared at $\sim9\times10^{13}$ W cm^{-2}. Figure 2a presents the signals of the 23rd, 25th and 27th harmonics, obtained at this intensity level, with respect to various nozzle

[1]Friedrich-Schiller-Universität Jena, Abbe Center of Photonics, Institute of Applied Physics, Albert-Einstein-Straße 15, 07745 Jena, Germany, [2]Helmholtz-Institute Jena, Fröbelstieg 3, 07743 Jena, Germany, [3]Ludwig-Maximilian-Universität München, Am Coulombwall 1, 85748 Garching, Germany, [4]Fraunhofer Institute for Applied Optics and Precision Engineering, Albert-Einstein-Straße 7, 07745 Jena, Germany. *e-mail: steffen.haedrich@uni-jena.de

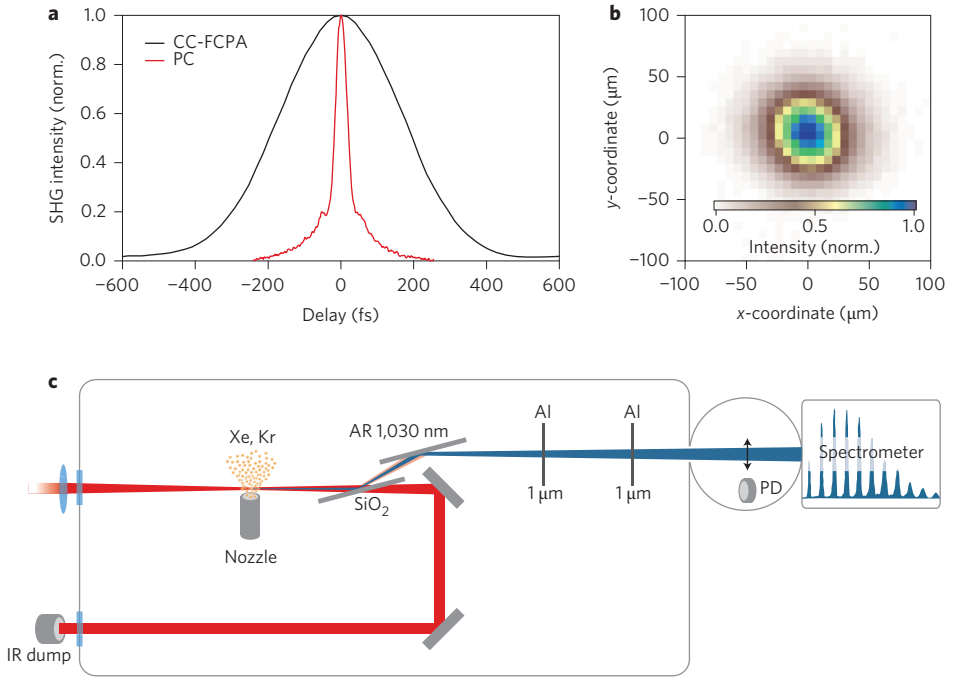

Figure 1 | Experimental set-up of the high harmonic generation experiments. a, The pulses of a fibre chirped pulse amplifier (CC-FCPA) are post-compressed (PC) (see Methods). Autocorrelation traces of the 340 fs (black) fibre laser and the 30 fs (red) compressed pulses are shown. The data is normalized (norm.). **b**, Intensity profile of the focal spot (diameter of 90 μm; $1/e^2$ intensity). **c**, Experimental set-up after the nonlinear compression stage, comprising a vacuum chamber used for the experiments on high harmonic generation. Pulses are focused (**b**) into a gaseous target (krypton, xenon) provided by simple cylindrical opening nozzles of various sizes (see main text). The generated harmonics co-propagate with the infrared beam and impinge on a chicane of two SiO_2 substrates under a 75° angle of incidence. Two aluminium filters (each of thickness 1 μm), isolate the harmonics, which are then sent into a flat-field grating spectrometer or onto a photodiode (PD) (see Methods).

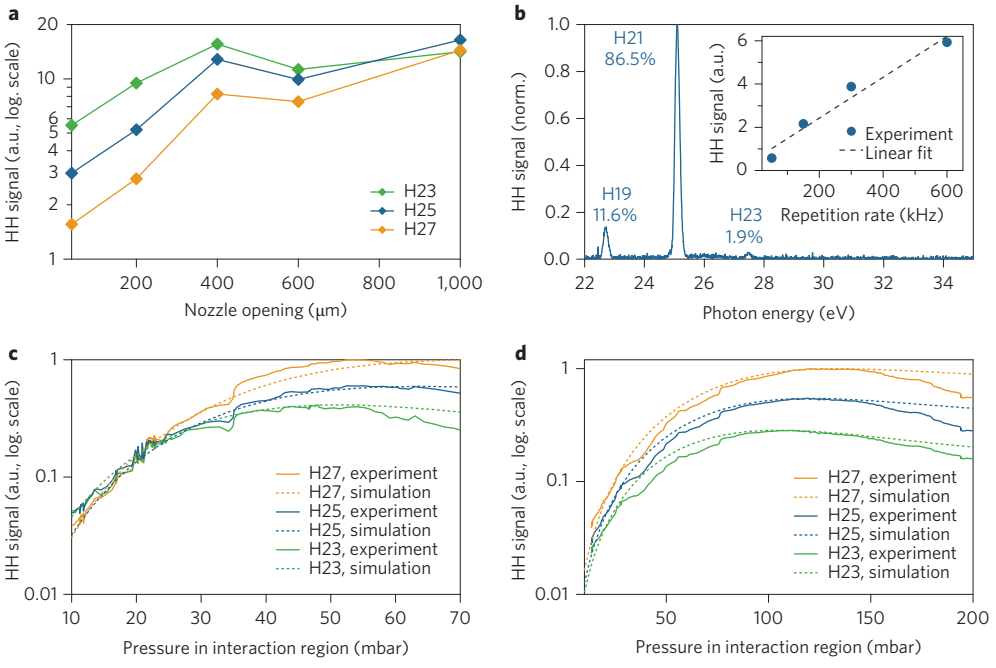

Figure 2 | Optimization and phase matching in high harmonic generation. a, Spatially and spectrally integrated signals (in arbitrary units (a.u.)) of three high harmonics (HHs; H23, H25 and H27) generated in xenon are shown with respect to nozzle opening size. **b**, Spectrum (blue curve) of the high harmonics transmitted through a 200 nm aluminium filter and a 200 nm zirconium filter, and respective percentages of the overall signal, as used for photodiode measurements (see main text and Methods). Inset: harmonic signal (sum over H21–H29) as a function of repetition rate. **c**, Signals of harmonics H23–H27 (solid lines) generated in a 1 mm xenon gas jet, recorded with respect to pressure. The results of a simulation (dashed lines, Supplementary Section II) are shown for an $I = 8 \times 10^{13}$ W cm^{-2}, 30 fs pulse. **d**, Signals of harmonics H23–H27 (solid lines) generated in a 600 μm krypton gas jet, recorded with respect to pressure. The results of a simulation (dashed lines, Supplementary Section II) are also shown for an $I = 9.7 \times 10^{13}$ W cm^{-2}, 30 fs pulse.

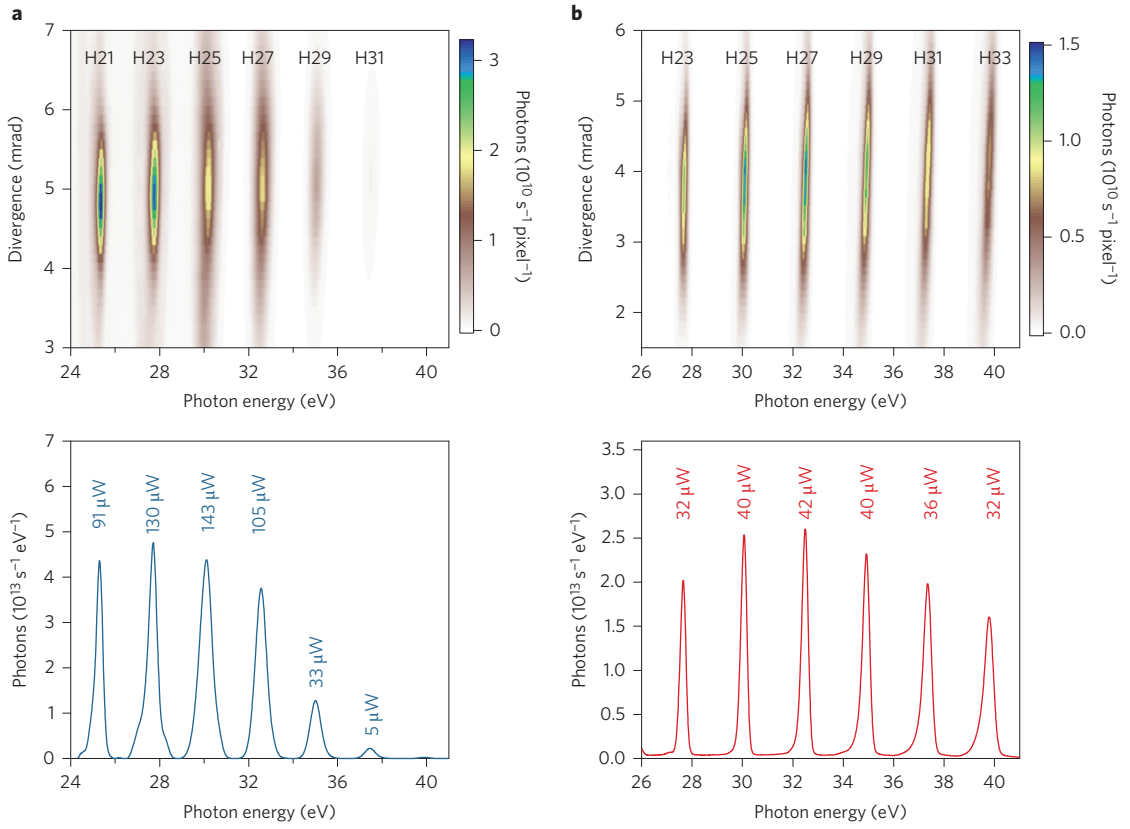

Figure 3 | High harmonic generation at a repetition rate of 0.6 MHz. a, Upper panel: spatial (*y*-axis) and spectral (*x*-axis) profiles of harmonics generated in a 1 mm xenon jet with the laser operated at a repetition rate of 0.6 MHz. Lower panel: spatial integration of the upper panel, together with the corresponding average power of each harmonic line. The strongest harmonic is H25 (30 eV) with an average power of 143 μW, corresponding to 3×10^{13} photons s^{-1}. **b**, Upper panel: spatial (*y*-axis) and spectral (*x*-axis) profiles of harmonics generated in a 600 μm krypton jet with the laser operated at a repetition rate of 0.6 MHz. Lower panel: spatial integration of the upper panel, together with the corresponding average power of each harmonic line. The strongest harmonic is H27 (32.5 eV) with an average power of 42 μW, corresponding to 8×10^{12} photons s^{-1}.

openings. Clearly, the signal increases up to the maximum opening diameter of 1 mm, where it starts to saturate. This behaviour is very similar for all observed harmonics (H19–H31), leading to broad plateau of strong harmonics. The absolute signal of the harmonics is obtained either with the known detection efficiency or with a photodiode (see Methods). The latter method was used to measure the average power of three harmonics (Fig. 2b) at 50 kHz, yielding values of 10.7 μW (H19), 13.3 μW (H21) and 15.5 μW (H23), which are in good agreement with our estimates (based on the known detection efficiency) of 8 μW (H19), 10 μW (H21) and 13 μW (H23), respectively. Because of this consistency between the two techniques, the photon flux for the remaining harmonics and for higher repetition rates was obtained using detection efficiencies. We also studied the phase-matching behaviour by varying the backing pressure of the gas jet and, simultaneously, recording the signal of the respective harmonics. The signal growth of the harmonics was also in good agreement with a numerical model[20,22] (Fig. 2c; see Supplementary Section I). According to a calculation with the Ammosov–Delone–Krainov (ADK) ionization model, the ionization fraction at the peak of the pulse is 24% and higher than the critical ionization level[21]. The experiment was therefore performed in a transient phase-matching regime, where the coherence length $L_{coh} = \pi/\Delta k$ is larger than the medium length over a short time interval at the rising edge of the pulse where the harmonics are generated and phase matching is achieved. The absorption lengths at optimal pressure (~60 mbar in the interaction region, Fig. 2c) are 590 μm (H23), 881 μm (H25), 1.1 mm (H27) and 2.4 mm (H31), which means that the lower-order harmonics are close to the absorption limit, and a longer interaction length would be required for higher orders[22] (Supplementary Section III). More importantly, the repetition rate of the laser system can be increased to 0.6 MHz (80 W of average power) with very similar pulse parameters (intensity, pulse duration and focal spot size), which is corroborated by the almost linear increase of the harmonic signal (Fig. 2b, inset). The spatial profiles and spatially integrated spectra for the experiments at 0.6 MHz are shown in Fig. 3a. The gas jet was positioned slightly behind the focus (~150 μm), which results in phase matching for the short trajectories, as indicated by the excellent spatial profiles of the low diverging harmonics[13]. A similar optimization was carried out for krypton gas targets (Fig. 2d), resulting in the use of a 600 μm nozzle placed ~180 μm behind the focus. The intensity of $\sim 9 \times 10^{13}$ W cm^{-2} (600 kHz) is similar, but the ionization is significantly reduced to <3% at the pulse peak. Consequently, phase matching can be achieved over an increased time window around the pulse peak, which results in spectrally narrower harmonics (Fig. 3b). In this case the coherence length is ~1 mm and the absorption lengths for an optimal pressure of 110 mbar are 162 μm (H23), 221 μm (H25), 286 μm (H27) and 730 μm (H33), which means, again, that the lowest harmonic orders are generated absorption-limited (Supplementary Section III). The obtained average power of the harmonics generated in xenon and krypton are shown in the lower panels of Fig. 3. Strong harmonics with more than 30 μW per harmonic, that is, more than 1×10^{12} photons s^{-1}, are obtained over a broad plateau extending from 25 eV to 40 eV. The highest average power is obtained for H25 (30 eV) with 143 μW, which corresponds to 3×10^{13} photons s^{-1} and a conversion efficiency of 1.8×10^{-6}. Experiments performed at a repetition rate of 300 kHz

and a different spectrometer configuration show that microwatt-level harmonics are generated up to H39 (47 eV). The achieved photon flux is within one order of magnitude of typical free-electron-laser operation[24], although these facilities can offer up to a few 10^{15} photons s^{-1} with high peak intensity[25].

In conclusion, we have demonstrated the most powerful source of coherent extreme-ultraviolet radiation (25–40 eV) enabled with HHG to date[6–8]. In combination with megahertz-level repetition rates, this will greatly advance applications in various fields, in particular in (multi)-dimensional surface science, coincidence detection experiments, photoelectron emission spectroscopy (PES) and microscopy (PEEM), (time-resolved) coherent diffractive imaging (CDI), among others[2,4,9,10]. Due to the excellent scaling properties of coherent combination, the availability of kilowatt-average-power femtosecond lasers[26] will further increase the HHG signal by another order of magnitude. Moreover, a second nonlinear compression stage can be implemented for achieving, potentially, sub-10 fs pulses with high average power and repetition rate. In combination with carrier-envelope phase stabilization this could also enable high-photon-flux megahertz isolated attosecond pulses[27]. Accordingly, the presented results are a major milestone towards new applications of coherent extreme-ultraviolet radiation in science and technology.

Methods

Fibre laser with nonlinear compression. The front end is an FCPA system that incorporates coherent combination (CC) of pulses from up to four main amplifier channels[28]. In the experiments presented here, the system was operated with a pulse energy of 270 μJ, a compressed pulse duration of ~340 fs and a repetition rate between 50 kHz and 0.6 MHz, which corresponds to an average power between 14 W and 163 W. Laser pulses were sent to the nonlinear compression set-up as described in ref. 23, and coupled into the 1.1-m-long hollow-core fibre (inner diameter of 250 μm). After evacuation, the tube was filled with 4 bar of krypton gas to enable spectral broadening. Subsequently, the pulses were compressed in time by a chirped mirror compressor with a group delay dispersion of –1,600 fs^2. After propagation through this set-up, the pulses were 29 fs short (Fig. 1a) with an energy of 130–150 μJ. At the highest repetition rate of 600 kHz, the average power used for HHG was >80 W.

HHG and characterization of extreme-ultraviolet radiation. The nonlinear compressed pulses were focused with an $f = 300$ mm lens (~f/50 focusing) onto a gaseous target inside a vacuum chamber. Simple cylindrical nozzles with different opening diameters (see main text) provided the gas targets. The generated harmonics and fundamental infrared laser co-propagated and impinged on a chicane of two SiO_2 substrates, which were used with an angle of incidence of 75° and p-polarization. The first substrate was pure fused silica and the second contained an anti-reflection coating (for infrared), with the top layer being SiO_2 (ref. 29). Consequently, the surfaces reflected the harmonics with sufficient efficiency (for example, ~17% at 30 eV for two reflections), and the infrared was suppressed to less than 1%. This allowed the following two aluminium filters to withstand even high-average-power operation. After the filters, the infrared light was completely suppressed and the harmonics were sent into a flat-field grating-based spectrometer (Ultrafast Innovations) equipped with a charge-coupled device (CCD) camera (Andor).

We used two independent methods to obtain the average power of individual harmonics. As described in the main text, the first method relies on filtering three harmonics (Fig. 2b) using a combination of a 200 nm aluminium filter and a 200 nm zirconium filter, and then measuring the average power with a photodiode (AXUV100G, Opto Diode). The measured current of the photodiode was converted into an average power with the known responsivity of the diode of 0.26 ± 0.01 A W^{-1} at 23–27 eV. This power was distributed among the harmonics according to the percentage values given in Fig. 2b. The harmonic signal before the filters was obtained using the measured transmission values of each filter and harmonic, respectively. The reflection coefficient of the SiO_2 surfaces was calculated using the general reflection coefficients[30] and the tabulated values for the complex refractive index of SiO_2 (ref. 31) in the extreme-ultraviolet range, which have shown good agreement with calibration measurements[29].

The second method is based on calculating the harmonic signal by accounting for the known efficiencies of the detection apparatus. The number of photons per second, $N_{ph,s}$, emitted directly after the gas jet was obtained with the equation

$$N_{ph,s} = \frac{S_{CCD} \cdot \sigma}{\eta_{QE} \cdot \left(E_{ph}/3.65\ \text{eV}\right) \cdot \eta_g \cdot t_{f1} \cdot t_{f2} \cdot R_p^2 \cdot t_{exp}}$$

where S_{CCD} is the measured signal (counts) on the detector, σ is the CCD sensitivity in electrons per count, η_{QE} is the quantum efficiency of the CCD, E_{ph} is the photon energy of the harmonics in eV (E_{ph}/3.65 eV is the number of electrons freed per photon at a bandgap energy of 3.65 eV), η_g is the grating diffraction efficiency, $t_{f1/2}$ are the filter transmissions, R_p is the reflection coefficient of a SiO_2 surface for p-polarized light, and t_{exp} is the exposure time. The CCD characteristics (σ, η_{QE}) were used as characterized by the manufacturer, the diffraction efficiency of the grating (η_g) was used as described in ref. 32, R_p was obtained as described above, and the transmission of the aluminium filters was measured. The so-obtained values have been compared to the photodiode measurement performed for harmonic orders H19, H21 and H23 and show good agreement (see main text).

One-dimensional model for HHG. We used a one-dimensional model to calculate the harmonic signal on-axis[20,22]. For that purpose we calculated the time-dependent wave-vector mismatch $\Delta k(t) = q \cdot k_0 - k_q$ according to our experimental conditions. This model proves very useful for understanding the phase-matching conditions present in our experiments. More details on the model and experimental conditions are presented in the Supplementary Information.

Received 17 March 2014; accepted 28 July 2014; published online 14 September 2014

References

1. Popmintchev, T., Chen, M.-C., Arpin, P., Murnane, M. M. & Kapteyn, H. C. The attosecond nonlinear optics of bright coherent X-ray generation. *Nature Photon.* **4,** 822–832 (2010).
2. Mathias, S. *et al.* in *Dynamics of Solid State Surface Interfaces* Vol. 1 *Current Developments* (eds Bovensiepen, U., Petek, H. & Wolf, M.) 499–535 (Wiley-VCH, 2010).
3. Südmeyer, T. *et al.* Femtosecond laser oscillators for high-field science. *Nature Photon.* **2,** 599–604 (2008).
4. Keller, U. Femtosecond to attosecond optics. *IEEE Photon. J.* **2,** 225–228 (2010).
5. Cingöz, A. *et al.* Direct frequency comb spectroscopy in the extreme ultraviolet. *Nature* **482,** 68–71 (2012).
6. Pupeza, I. *et al.* Compact high-repetition-rate source of coherent 100 eV radiation. *Nature Photon.* **7,** 608–612 (2013).
7. Rundquist, A. *et al.* Phase-matched generation of coherent soft X-rays. *Science* **280,** 1412–1415 (1998).
8. Brichta, J.-P. *et al.* Comparison and real-time monitoring of high-order harmonic generation in different sources. *Phys. Rev. A* **79,** 033404 (2009).
9. Sansone, G., Calegari, F. & Nisoli, M. Attosecond technology and science. *IEEE J. Sel. Top. Quantum Electron.* **18,** 507–519 (2012).
10. Sandberg, R. L. *et al.* Lensless diffractive imaging using table-top coherent high-harmonic soft-X-ray beams. *Phys. Rev. Lett.* **99,** 098103 (2007).
11. McPherson, A. *et al.* Studies of multiphoton production of vacuum-ultraviolet radiation in the rare gases. *J. Opt. Soc. Am. B* **4,** 595–601 (1987).
12. Ferray, M. *et al.* Multiple-harmonic conversion of 1064 nm radiation in rare gases. *J. Phys. B* **21,** L31 (1988).
13. Salières, P., L'Huillier, A. & Lewenstein, M. Coherence control of high-order harmonics. *Phys. Rev. Lett.* **74,** 3776–3779 (1995).
14. Antoine, P., L'Huillier, A. & Lewenstein, M. Attosecond pulse trains using high-order harmonics. *Phys. Rev. Lett.* **77,** 1234–1237 (1996).
15. Corkum, P., Burnett, N. & Ivanov, M. Y. Subfemtosecond pulses. *Opt. Lett.* **19,** 1870–1872 (1994).
16. Allison, T. K., Cingöz, A., Yost, D. C. & Ye, J. Extreme nonlinear optics in a femtosecond enhancement cavity. *Phys. Rev. Lett.* **107,** 183903 (2011).
17. Vernaleken, A. *et al.* Single-pass high-harmonic generation at 20.8 MHz repetition rate. *Opt. Lett.* **36,** 3428–3430 (2011).
18. Corkum, P. B. Plasma perspective on strong field multiphoton ionization. *Phys. Rev. Lett.* **71,** 1994–1997 (1993).
19. Lewenstein, M., Balcou, P., Ivanov, M. Y., L'Huillier, A. & Corkum, P. B. Theory of high-harmonic generation by low-frequency laser fields. *Phys. Rev. A* **49,** 2117–2132 (1994).
20. Kazamias, S. *et al.* Pressure-induced phase matching in high-order harmonic generation. *Phys. Rev. A* **83,** 063405 (2011).
21. Paul, A. *et al.* Phase-matching techniques for coherent soft X-ray generation. *IEEE J. Quantum Electron.* **42,** 14–26 (2006).
22. Constant, E. *et al.* Optimizing high harmonic generation in absorbing gases: model and experiment. *Phys. Rev. Lett.* **82,** 1668–1671 (1999).
23. Hädrich, S. *et al.* Nonlinear compression to sub-30 fs, 0.5 mJ pulses at 135 W of average power. *Opt. Lett.* **38,** 3866–3869 (2013).
24. Epp, S. *et al.* Soft X-ray laser spectroscopy on trapped highly charged ions at FLASH. *Phys. Rev. Lett.* **98,** 183001 (2007).
25. Ackermann, W. *et al.* Operation of a free-electron laser from the extreme ultraviolet to the water window. *Nature Photon.* **1,** 336–342 (2007).
26. Limpert, J. *et al.* Performance scaling of ultrafast laser systems by coherent addition of femtosecond pulses. *IEEE J. Sel. Top. Quantum Electron.* **20,** 1–10 (2014).
27. Krebs, M. *et al.* Towards isolated attosecond pulses at megahertz repetition rates. *Nature Photon.* **7,** 555–559 (2013).

28. Klenke, A. *et al.* 530 W, 1.3 mJ, four-channel coherently combined femtosecond fiber chirped-pulse amplification system. *Opt. Lett.* **38,** 2283–2285 (2013).
29. Pronin, O. *et al.* Ultrabroadband efficient intracavity XUV output coupler. *Opt. Express* **19,** 10232 (2011).
30. Attwood, D. *Soft X-Rays and Extreme Ultraviolet Radiation: Principles and Applications* (Cambridge Univ. Press, 1999).
31. Philipp, H. R. in *Handbook of Optical Constants of Solids*, Vol. I (ed. Palik, E. D.) 749–763 (Academic Press, 1997); http://dx.doi.org/10.1016/B978-012544415-6.50038-8
32. Demmler, S. *et al.* Generation of high-photon flux-coherent soft X-ray radiation with few-cycle pulses. *Opt. Lett.* **38,** 5051–5054 (2013).

Acknowledgements

This work was partly supported by the German Federal Ministry of Education and Research (BMBF) and the European Research Council under the European Union's Seventh Framework Programme (FP7/2007-2013)/ERC (grant agreement no. 240460). A.K. acknowledges financial support from the Helmholtz-Institute Jena.

Author contributions

J.L., S.H., J.R. and M.K. conceived the experiment. The experiments were planned and performed by S.H., J.R., A.K., A.H. and M.K. Data were analysed by S.H. with support from J.R. and M.K. All authors discussed and contributed to interpretation of the results. J.L. and A.T. supervised the project and acquired funding. The idea for and design of the anti-reflection-coated SiO_2 substrates originate from O.P. and V.P., who also fabricated the samples used in this experiment. All authors contributed to writing the manuscript.

Additional information

Supplementary information is available in the online version of the paper. Reprints and permissions information is available online at www.nature.com/reprints. Correspondence and requests for materials should be addressed to S.H.

Competing financial interests

The authors declare no competing financial interests.